T Lymphocytes and Cytotoxic Astrocyte Blebs Correlate across Autism Brains

Marcello M. DiStasio, MD, PhD,[1] Ikue Nagakura, PhD,[1] Monica J. Nadler, PhD,[1] and Matthew P. Anderson, MD, PhD [1,2,3]

Objective: Autism spectrum disorder (ASD) affects 1 in 59 children, yet except for rare genetic causes, the etiology in most ASD remains unknown. In the ASD brain, inflammatory cytokine and transcript profiling shows increased expression of genes encoding mediators of the innate immune response. We evaluated postmortem brain tissue for adaptive immune cells and immune cell–mediated cytotoxic damage that could drive this innate immune response in the ASD brain.
Methods: Standard neuropathology diagnostic methods including histology and immunohistochemistry were extended with automated image segmentation to quantify identified pathologic features in the postmortem brains.
Results: We report multifocal perivascular lymphocytic cuffs contain increased numbers of lymphocytes in ~65% of ASD compared to control brains in males and females, across all ages, in most brain regions, and in white and gray matter, and leptomeninges. $CD3^+$ T lymphocytes predominate over $CD20^+$ B lymphocytes and $CD8^+$ over $CD4^+$ T lymphocytes in ASD brains. Importantly, the perivascular cuff lymphocyte numbers correlate to the quantity of astrocyte-derived round membranous blebs. Membranous blebs form as a cytotoxic reaction to lymphocyte attack. Consistent with multifocal immune cell–mediated injury at perivascular cerebrospinal fluid (CSF)–brain barriers, a subset of white matter vessels have increased perivascular space (with jagged contours) and collagen in ASD compared to control brains. CSF–brain barrier pathology is also evident at cerebral cortex pial and ventricular ependymal surfaces in ASD.
Interpretation: The findings suggest dysregulated cellular immunity damages astrocytes at foci along the CSF–brain barrier in ASD.

ANN NEUROL 2019;86:885–898

Autism spectrum disorder (ASD) manifests in early childhood and is diagnosed based on behavioral deficits including impaired social and increased repetitive behaviors and restricted interests. The study of ASD postmortem brain tissue provides insights into the pathologic processes that underlie this disorder currently defined exclusively by behavioral deficits. Using ASD human postmortem brain tissues, investigators have discovered an increase of cytokines, chemokines, growth factors, and activated astroglia and microglia in the cerebral cortex, white matter, and cerebellum in ASD, indicating ongoing activity of the innate immune system.[1–5] Genome-wide transcriptional profiling has revealed an increase in the expression of a diverse array of genes encoding mediators of this activated innate immune response along with an overall decrease in the expression of many neuron-related genes.[6–8] Here, we applied computer vision algorithms to quantify astrocyte-derived round membranous blebs, multifocal perivascular lymphocytic cuffs, and increased perivascular space and collagen, novel neuropathologic features that we found in a large proportion of ASD brains. The results provide the signatures of a cellular immune response, reflected by T-lymphocyte infiltrates and cytotoxic cell injuries (typical of T lymphocytes) to cerebrospinal fluid (CSF)–brain barrier astrocytes, in ASD compared to control postmortem brains.

Materials and Methods

Study Subjects

The study was approved by the institutional review board of the Beth Israel Deaconess Medical Center. Cases were selected from the Autism Tissue Program and Autism BrainNet brain banking programs and from the neuropathology archives of the Beth Israel

View this article online at wileyonlinelibrary.com. DOI: 10.1002/ana.25610

Received Nov 21, 2018, and in revised form Sep 24, 2019. Accepted for publication Sep 25, 2019.

Address correspondence to Dr Anderson, 330 Brookline Ave, E/CLS-645, Boston, MA 02215. E-mail: Matthew_Anderson@bidmc.harvard.edu

From the [1]Departments of Neurology and Pathology, Beth Israel Deaconess Medical Center; [2]Boston Children's Hospital Intellectual and Developmental Disabilities Research Center; and [3]Program in Neuroscience, Harvard Medical School, Boston, MA

Additional supporting information can be found in the online version of this article.

© 2019 American Neurological Association

Deaconess Medical Center in Boston, Massachusetts. We analyzed postmortem brain tissues from 25 ASD and 30 control cases. All tissues were from postmortem cases with informed consent obtained from the next of kin. ASD and control cases with age at death <70 years were reviewed. Exclusion criteria were evidence of a central nervous system (CNS) infection, neurodegenerative disease, or other neuropsychiatric disorder where ASD was absent, and additionally for control cases, a known family member with ASD. A history of seizures was documented in 13 of 25 (52%) ASD and 8 of 30 (27%) control cases. Additional clinical and other case data, including brain weight, are shown in the Supplementary Table. One of the control cases, C18, had a mutation in *CDKL5* and early infantile epileptic encephalopathy. ASD cases include those with known point mutations in A1, A2, and A3, XYY karyotype in A4, and chromosome 15q duplication in A5.

Histology and Immunohistochemical Staining

The brain region sample distribution was similar for ASD and control cases. Samples were processed following standard histologic methods; following formalin fixation and paraffin embedding, tissue blocks were cut into 5μm-thick sections for all samples, mounted on glass slides, and stained with hematoxylin and eosin and Luxol fast blue (H&E + LFB). All available blocks containing cerebral cortex were also used for Masson trichrome staining (collagen). Following automated lymphocyte quantification (see below), blocks from each case (ASD and control) with the highest lymphocyte counts were selected for staining with primary antibodies raised against CD3, CD20, CD4, and CD8 using avidin–biotin immunohistochemistry. Standard immunohistochemical staining protocols were followed, using 5μm-thick sections taken from the formalin-fixed paraffin-embedded tissue blocks. A single antibody per slide was applied to sequential sections from the blocks. The block from each case with the largest median perivascular space identified on H&E was selected for staining with glial fibrillary acidic protein (GFAP) and CD68. Blocks from selected autism cases with the largest median perivascular space were additionally stained with S100b and ALDH1L1. Control staining was performed for all primary antibodies used in the study and did not show background staining.

Automated Lymphocyte Detection and Segmentation Procedure

All available H&E + LFB-stained slides were reviewed with a standard bright field microscope, and photographs were taken using a × 60 objective (×600 total magnification, TIFF format, resolution = 2,448 × 1,920 pixels) using a 5-megapixel charge-coupled device camera (Model DP27; Olympus, Tokyo, Japan). On every H&E + LFB-stained section from every ASD and control case, while blinded to the diagnosis, we photographed 3 blood vessels with the most abundant perivascular lymphocytes in each of the following brain compartments: gray matter, white matter, and leptomeninges. Fields containing single vessels (luminal diameter range = 15–500μm) involved by the highest density of lymphocytes were selected from ASD and control cases using a × 40 objective. This resulted in a collection of images with identical field of view sizes.

All images were then analyzed using a custom-built program in MATLAB (MathWorks, Natick, MA) to perform the following operations: convert the original RGB image to HSV color space; smooth the hue channel using a Gaussian kernel with $\sigma = 80$, and then threshold around the largest hue peak between (0.55, 0.8) to create a mask for white matter; smooth the value channel using a Gaussian kernel with $\sigma = 5$, and apply an Otsu automatic threshold; to eliminate white matter oligodendroglia from further analysis, apply the inverse of the white matter mask to the smoothed value channel; next, apply the morphologic opening operation, followed by watershed segmentation; then, erode with a disc structuring element (4-pixel diameter); delete regions with areas outside lymphocyte size range as expected for the known image magnification; delete regions for which $(4 \times \pi \times \text{area}) / \text{perimeter}^2 < 0.5$ (to loosely enforce circularity); apply the circular Hough transform algorithm for circle identification (radius range = 10–20 pixels, sensitivity = 0.99, edge gradient threshold = 0.95); finally, threshold circle regions on the mean of the saturation channel; return a list of statistics for each circular region of interest (ROI): area, centroid, eccentricity, mean intensity, and perimeter.

All circular ROIs were marked on H&E + LFB images, with their mean saturations. All output images were manually reviewed for accuracy, and if cell nuclei were misidentified as lymphocytes or if lymphocyte nuclei were missed, cell counts for the images were manually corrected. This procedure resulted in identification of 29,549 lymphocytes involving 1,868 vessels across 9 brain regions in the entire study set.

Automated White Matter Perivascular Space Segmentation Procedure

All available H&E + LFB-stained slides were reviewed with a standard bright field microscope with camera, as described above. The 10 white matter vessels surrounded by the largest space intervening between the vessel wall and white matter parenchyma were selected from ASD and control cases using a × 20 objective and photographed (×200 total magnification).

All images were analyzed using a custom-built program in MATLAB to perform the following operations: downsample image by a factor of 4; color threshold RGB image to find LFB-stained regions (based on a composite example LFB image); morphologic close with 4-pixel radius disk element; fill holes and apply resulting mask to original RGB image, convert to Lab color space; apply contrast-limited adaptive histogram equalization to "B" channel using 64 tiles; convert to grayscale; subtract smoothed version of image (Gaussian kernel, sigma = 16 pixels); apply an Otsu threshold, and apply a morphologic closing operation.

The resulting ROI was taken as the mask whose edges were defined by the boundary of the LFB staining around the photographed vessel. This ROI served as the basis for area and boundary contour measurements.

Automated Trichrome Perivascular Collagen Segmentation Procedure

Trichrome-stained slides created from all available blocks containing cerebral cortex were reviewed with a standard bright field microscope and camera using a × 20 objective, as described above. Six blood vessels in white matter surrounded by the largest amount of blue-stained perivascular collagen among all blocks

for each ASD and control case were photographed using a × 20 objective (×200 total magnification).

All images were then analyzed using a custom-built MATLAB program to perform the following operations: downsample image by a factor of 4 and convert to Lab color space; z score "a" and "b" channels; threshold color based on distance in "ab" space from a defined center color (<1.75 from [−6, 1]); apply image dilation and morphologic opening to resulting mask, and fill holes; find boundaries in mask, retain regions enclosed by boundaries that are connected to the most central region by a space no more than 2% of the image width (Dijkstra algorithm), to eliminate any blue-staining regions not associated with the vessel of interest; fill holes, and apply an erode mask using a 12-pixel diameter disk element.

This provided a coarse mask for the blue-staining collagen in the images. A second color threshold based on distance to the center in color space was then applied within this coarse mask applied to the Lab image, and the result was used for the final measurement of collagen area. The largest enclosed area inside the coarse mask (ie, largest hole in the mask) after a dilation by a 12-pixel diameter disk element was taken as the lumen area and used as a normalization for the collagen area.

Immunohistochemistry Image Acquisition and Analysis

Using a × 40 objective (×400 total magnification), we photographed 10 of the white matter blood vessels with the most abundant perivascular GFAP debris signal across all blocks containing cerebral cortex in each of the ASD and control cases to quantify perivascular GFAP$^+$ debris in white matter. MATLAB software was used to deconvolve the 3,3′-diaminobenzidine color channel, smooth it, threshold it, and measure the total positively stained area after manual masking of surrounding positively stained material in the brain parenchyma.

CD3-stained slides were imaged on a whole-slide scanning system using raster scan following manual focal point selection. The resulting whole-slide images were analyzed using a combination of direct cell density measurement with QuPath histology image analysis software[9] and a custom-written program in Python using the ImageJ libraries to process images tile by tile after import with the BioFormats plugin. After color deconvolution to separate the 3,3′-diaminobenzidine–stained regions, images were smoothed and thresholded, followed by morphologic opening, erosion, and watershed segmentation, after which the ImageJ particle analyzer was used to identify stained regions with size >12μm and circularity in the range of 0.4 to 1.0.

CD4-, CD8-, and CD20-stained slides were manually reviewed, and the 10 fields of view (×40 objective, ×400 total magnification) containing the highest cell counts for ASD and control cases were photographed. Lymphocytes (CD4, CD8, and CD20 stains) were manually counted.

We photographed at ×100 total magnification 5 of the white matter blood vessels with the most abundant perivascular space CD68 signal in each ASD and control case and quantified the number and cytoplasmic area of CD68$^+$ cells. The CD68 images were additionally quantified using MATLAB software to deconvolve the 3,3′-diaminobenzidine color channel, smooth it, threshold it, and measure the total positively stained area.

Statistical Methods

All images were analyzed using custom-designed algorithms implemented in MATLAB as described above. Cells and tissue structures of interest were segmented on all images, and all segmentation results were validated by manual inspection by 2 pathologists. The segmented regions of interest were the basis for morphologic measurements on each area, including cell counts, areas, perimeters, and jaggedness (squared second derivative of perimeter contour). Statistical inferences for continuous variables were made using Welch t tests, analysis of variance with Tukey post hoc comparison of means, simple linear regression, Kendall rank-order correlation for non-normally distributed variables, and receiver operating characteristic (ROC) curves, all implemented in R.

Results

Damage of CSF–Brain Barrier Astrocyte Processes in ASD

We observed a unique histologic feature in the perivascular Virchow–Robin CSF spaces of some of the small-caliber blood vessels in the brain from some individuals with ASD that was absent from the controls: round and uniformly eosinophilic membranous blebs of varying sizes (see H&E + LFB-stained sections in Fig 1A). These membranous blebs (pale blue in Fig 1B) were often in proximity to CD8$^+$ lymphocytes. Immunohistochemistry for astrocyte marker GFAP revealed strong positive staining of the membranous blebs, with some blebs contiguous with long narrow astrocytic processes (see Fig 1). The membranous blebs also stained positive for 2 additional astrocyte markers, S100B and ALDH1L1, confirming their astrocyte origins. In photomicrographs of white matter blood vessels visually chosen for the most abundant GFAP$^+$ material in each ASD and control case, the area occupied by the perivascular astrocyte blebs (defined as GFAP$^+$ area within the space delimited by the vascular endothelium and white matter edge/glia limitans) was markedly increased in ASD relative to controls. To rule out an artifact due to postmortem tissue disintegration, cases in which the thin GFAP$^+$ astrocyte processes of the white and gray matter had degraded (fine fibrillary structures lost) were excluded from the analysis. Using the same sampling strategy on sections stained for the macrophage marker CD68, we found an increase in the area of cytoplasmic staining but no increase in total number of CD68$^+$ macrophages in ASD compared to controls in these white matter perivascular spaces (not shown). Reactive microglia were also observed in ASD, but not quantified.

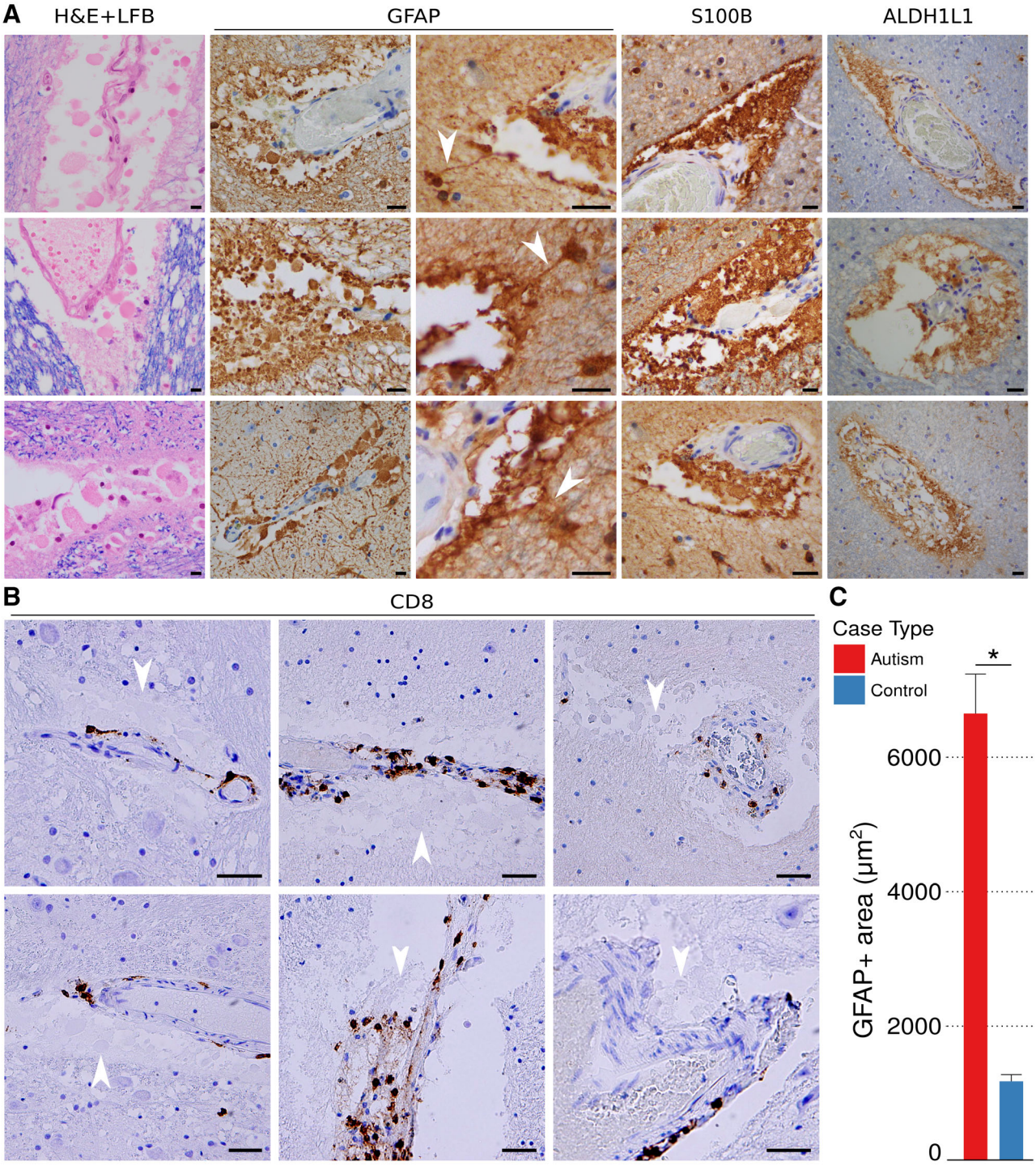

FIGURE 1: Perivascular membranous blebs stain with multiple astrocyte markers and colocalize with CD8$^+$ T cells in autism spectrum disorder (ASD) brains. (A) Round and uniformly eosinophilic membranous blebs of varying sizes were identified in the perivascular Virchow–Robin spaces of autism brains (white matter examples; all scale bars = 40μm). The membranous blebs are eosinophilic on hematoxylin and eosin and Luxol fast blue (H&E + LFB; column 1). Glial fibrillary acidic protein (GFAP), S100, and ALDH1L1 immunohistochemical staining (columns 2–4) establishes the blebs as derived from astrocytes. (B) Photomicrographs taken from gray and white matter samples from ASD brain cases double stained by immunohistochemistry for CD8 and hematoxylin reveal the cytotoxic CD8$^+$ T cells (brown) in close proximity to membranous blebs (pale blue, *arrowheads*; all scale bars = 40μm). (C) Perivascular GFAP$^+$ material was increased in autism compared to controls ($n_{vessels}$[autism] = 209, $n_{vessels}$[control] = 120). Bar heights represent mean, and whiskers represent standard error of the mean. *$p < 0.05$, Welch *t* test.

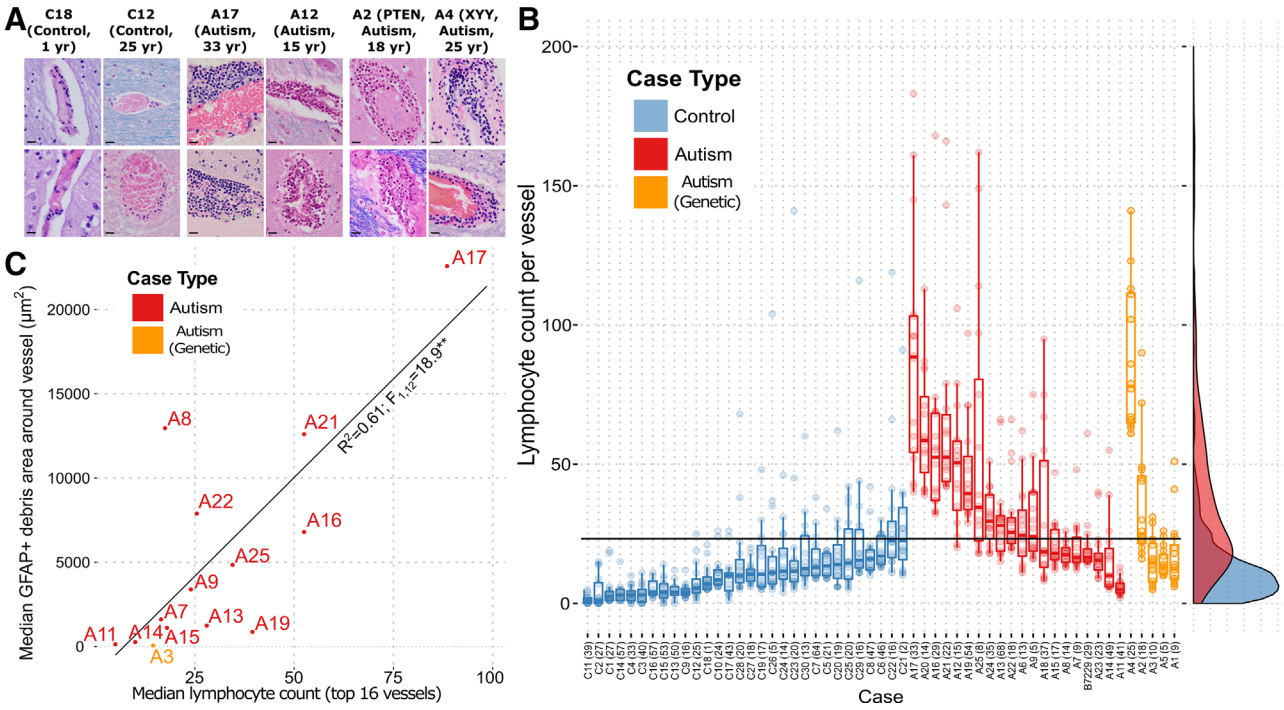

FIGURE 2: Lymphocytes are increased in cuffs around a subset of vessels, and their numbers correlate to the quantity of perivascular glial fibrillary acidic protein (GFAP)$^+$ membranous blebs across autism spectrum disorder (ASD) cases. (A) Representative images of blood vessels in the brain parenchyma of 2 control patients and 4 patients carrying an autism diagnosis show increased abundance of aggregated perivascular lymphocytes in the autism cases (all scale bars = 40μm). (B) Perivascular lymphocyte counts for each of the top vessels (up to 16) in every case identified by comprehensive visual inspection of the slides show an increase in ASD compared to control cases. Dots represent lymphocyte counts for each vessel. Overlaid box-and-whisker plots represent the median, upper and lower quartile, and upper/lower quartile ±1.5*(interquartile range). Smoothed density plots for all cases are shown on the right margin. X-axis labels are case names, with years of age in parentheses. The horizontal black cutoff line represents the lymphocyte count of 23 that gives the highest sensitivity for autism versus control while preserving 95% specificity. The aggregate differences between autism and control counts are statistically significant ($p < 0.0005$; analysis of variance with Tukey post hoc comparison of means), as are the difference between genetic autism and control ($p < 0.0005$), but not the difference between autism and genetic autism ($p = 0.098$; $n_{vessels}$[autism] = 336, $n_{vessels}$[control] = 272, $n_{vessels}$[genetic autism] = 64). (C) A plot of perivascular GFAP$^+$ debris against perivascular lymphocyte counts (top up to 16 vessels) for each case shows the correlation between astrocyte-derived debris and lymphocyte numbers. **$p < 0.001$ for linear regression; the rank-order correlation has a Kendall tau of 0.51 ($p = 0.01$).

CD8$^+$ Cytotoxic T Lymphocytes Are Increased in ASD

Microscopic visual inspection of H&E + LFB-stained brain sections revealed rare but prominent perivascular lymphocytic cuffs scattered in a semirandom pattern across the brain tissue blocks that were more numerous and prominent in ASD than control brains. This clinical assessment was confirmed using segmentation algorithms with manually tuned parameters (lymphocytes defined by shape and color on H&E). The number of lymphocytes in the most populated perivascular cuffs, visually identified and photographed from each ASD and control case, was increased in ASD compared to controls in gray matter, white matter, and leptomeninges (Figs 2 and 3), in the gray and white matter of both male and female subjects, across all studied age groups, and in most brain regions (see Fig 3). Among the most involved brain parenchymal blood vessels identified in both ASD and control for each case, the lymphocyte count per vessel was 15.0 ± 0.6 in ASD and 5.8 ± 0.4 in controls (mean ± standard error of the mean). This difference of means yields $p < 0.01$ by Welch t test (statistical significance was also found with a linear mixed-effects model fit). The number of perivascular lymphocytes did not correlate with the history of seizures (see Fig 3D, E). When measured across whole slide scanned images containing large regions of cortex and white matter, CD3$^+$ T-lymphocyte densities were increased in ASD relative to control (Fig 4A–C, B inset). Lymphocyte counts were increased in 64% of the autism cases (see Fig 2B), including in 2 cases with known genetic defects (*PTEN* and XYY), when using the top 16 blood vessels with the highest lymphocyte counts in each ASD and control case and a median count of 23 lymphocytes that exceeded the control threshold (parameters chosen to yield ≥95% specificity; area under ROC curve = 0.785). Immunohistochemistry revealed that the

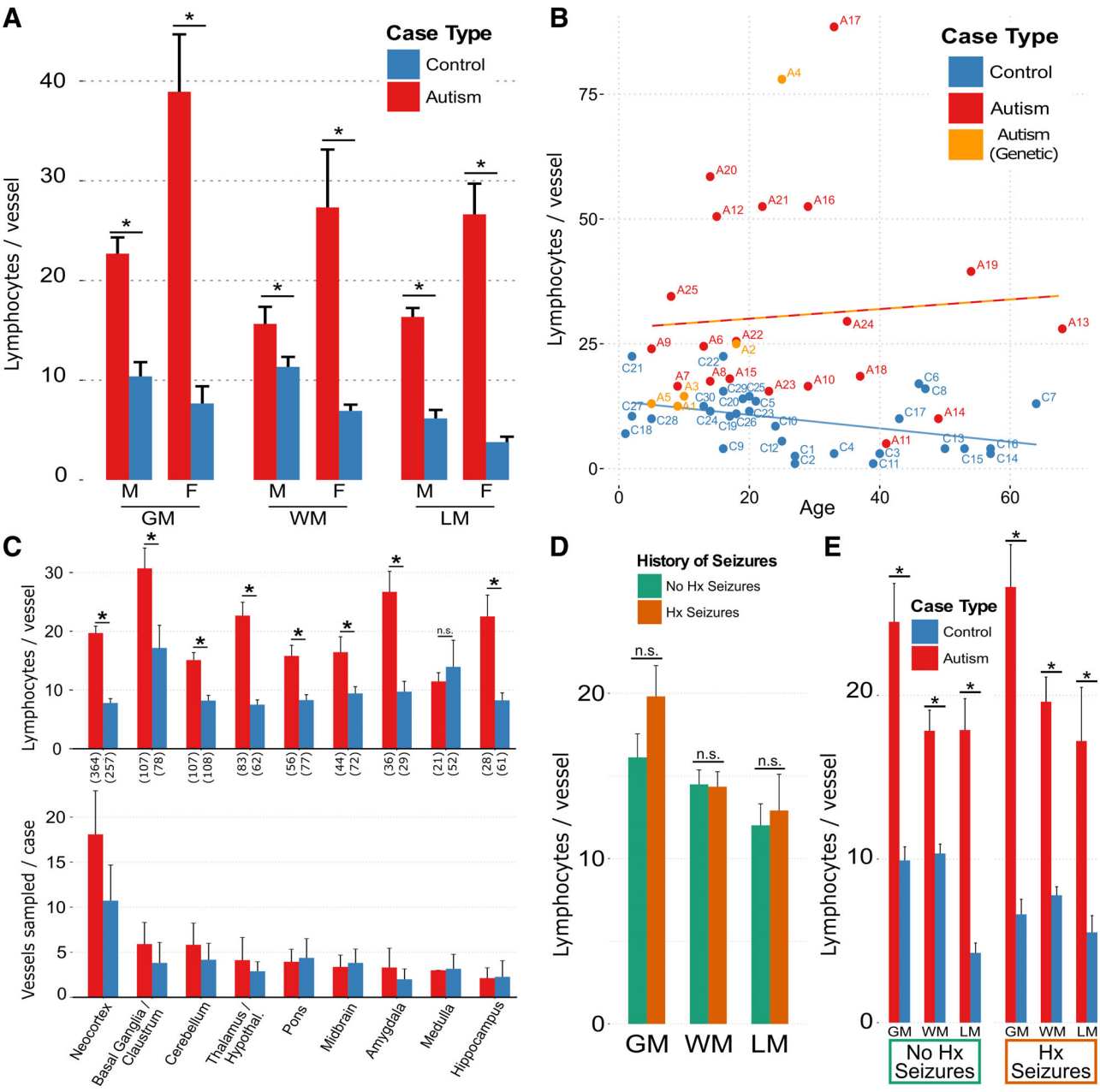

FIGURE 3: Perivascular cuff lymphocytes are increased across brain regions, compartments, and ages in autism spectrum disorder. (A) Perivascular lymphocyte counts in gray matter (GM), white matter (WM), and leptomeningeal (LM) compartments, separated by sex; *$p < 1^{e-15}$, multilinear regression (MLR) for control versus autism, controlling for sex and compartment. F = female; M = male. (B) Median perivascular lymphocyte counts among the top 16 vessels for each case, plotted by age in years for autism, control, and genetic autism cases, show that an increase in autism relative to control. The 2 lines in B represent a linear regression of lymphocyte count versus age for control (blue) and autism (red-orange; includes genetic autism) and show a separation of the groups, with a diverging upward trend for autism and downward trend for controls of lymphocyte number with increasing age. (C) Top: Perivascular lymphocyte counts across brain regions were higher in all regions except for medulla in autism (including genetic autism) cases compared with control cases (*$p < 0.05$, Welch *t* test; n.s. = not significant). Numbers of sampled vessels across all cases are in parentheses along the abscissa. Bottom: Sampling of vessels in this study was similar across brain regions for autism compared with control cases. The mean ± standard error of the mean (s.e.m.) total number of vessels sampled per case was 42.6 ± 10.9 for autism cases and 25.8 ± 15.1 for control cases. Bar heights and whiskers represent mean ± s.e.m. number of vessels sampled per case from each brain region for autism and control cases. (D, E) The effect of history of (Hx) seizures on perivascular lymphocyte count in autism and control cases was not sufficient to explain the observed difference in lymphocyte counts (*$p < 0.05$, Welch *t* test; n.s. = not significant). In an MLR prediction of number of lymphocytes, it was found that case type (autism or control) was a significant predictor ($\beta = 14.5$, $p < 1^{e-15}$), but history of seizures ($\beta = 2.3$, $p = 0.07$) and the interaction between autism and seizure history ($\beta = 0.7$, $p = 0.76$) were not. Bar heights in all panels represent mean, whiskers represent s.e.m. For all panels, $n_{vessels}$(autism) = 846, $n_{vessels}$(control) = 796.

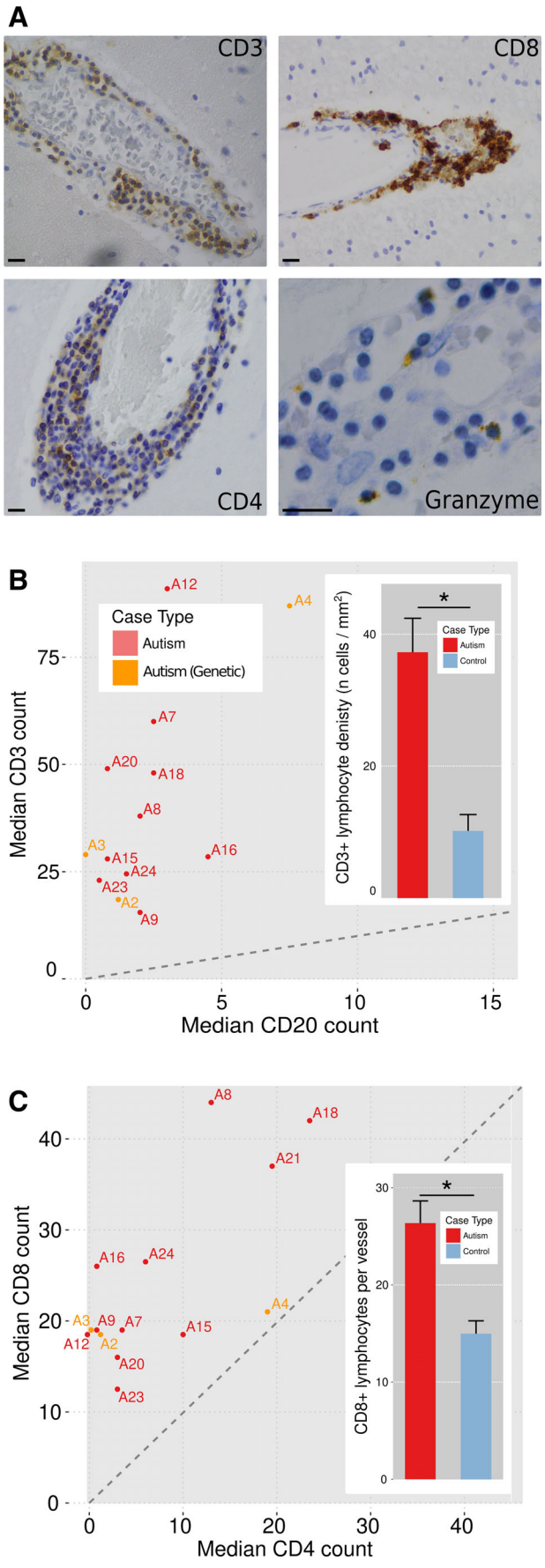

immune cells are predominantly $CD3^+$ and $CD8^+$ T lymphocytes (see Fig 4B, C), along with a smaller population of $CD4^+$ T cells and fewer small clusters of $CD20^+$ B cells. A subset of lymphocytes contained granzyme B^+ cytoplasmic puncta, a T-lymphocyte and NK cell proteolytic effector molecule (see Fig 4A).

Quantities of Lymphocytes and Astrocyte Debris Correlate across ASD Cases

Importantly, comparison at the case level revealed that the quantity of perivascular $GFAP^+$ debris (median of the 10 most involved vessels; includes the membranous blebs) correlates to the number of lymphocytes (median of the 16 vessels most involved by lymphocyte cuffs) across ASD cases (see Fig 2C).

Perivascular Space Is Increased and Has a More Jagged Contour in ASD

Based on the perivascular distribution of lymphocytes and cell debris and our histologic observation of foci with enlarged perivascular spaces and prominent adventitial collagen in the ASD cases, we performed quantitative measures of these features where most prominent (hereafter referred to as top vessels) in ASD and control cases. Perivascular space, like lymphocyte numbers, was increased around vessels in ASD relative to control when comparing the top 10 vessels (Fig 5), including in the genetic form $PTEN^{+/-}$ (Case A2). We also observed a jagged contour to the edge of the perivascular white matter surrounding these top vessels that was increased in ASD relative to control (quantified using a squared second derivative of the contour, designated jaggedness; see Fig 5), consistent with a segmental cell-mediated damage of perivascular astrocytes. Increased jaggedness was also observed selectively in the 2 genetic cases of ASD with increased lymphocytes (XYY [Case A4] and

FIGURE 4: $CD8^+$ cytotoxic T lymphocytes predominate in the focal perivascular cuffs in autism spectrum disorder (ASD) brains. (A) Representative photomicrographs of CD3, CD8, CD4, and granzyme B immunohistochemically stained perivascular lymphocytic cuffs in autism cases. (B) Comparison of the median per-vessel $CD3^+$ and $CD20^+$ lymphocyte counts for the autism cases and a comparison of mean ± standard error of the mean (s.e.m.) density of total $CD3^+$ count across whole slides for autism and control cases (*inset*; n_{cases}[autism] = 18, n_{cases}[control] = 21; *$p < 0.001$). ASD cases fall above the diagonal *(dashed line)*, indicating $CD3^+$ T-cell predominance. (C) Comparison of the median per-vessel $CD8^+$ and $CD4^+$ lymphocyte counts for the autism cases and a comparison of mean ± s.e.m. perivascular $CD8^+$ lymphocyte counts for the autism and control cases (*inset*; $N_{vessels}$[autism] = 66, $N_{vessels}$[control] = 62; *$p < 0.001$). ASD cases fall above the diagonal, indicating $CD8^+$ cytotoxic T-cell predominance.

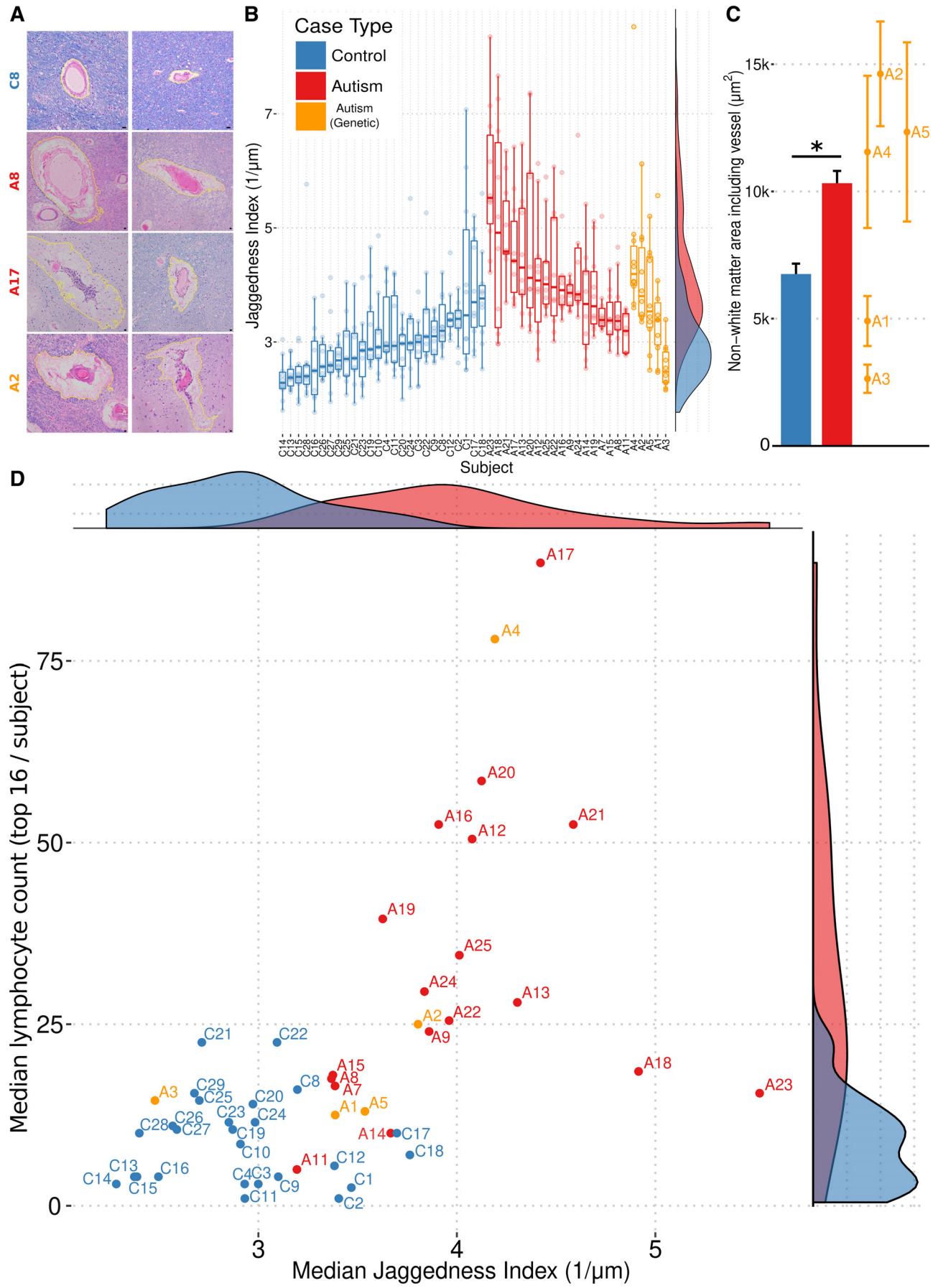

(Figure legend continues on next page.)

PTEN$^{+/-}$ [Case A2]). Control and ASD cases are robustly separated in a scatterplot of median perivascular lymphocyte count and median jaggedness index of the top vessels (see Fig 5D), suggesting that combined use of these 2 parameters better separates ASD from control.

Perivascular Fibrosis Is Increased in ASD

The quantity of perivascular collagen was evaluated by staining with trichrome and measured as the area of blue-stained collagen normalized to vessel lumen area for the 6 vessels with the most prominent collagen in ASD and control cases (see examples, Fig 6A). Adventitial perivascular collagen was increased at these top vessels from ASD relative to control (see Fig 6B), including in ASD with *PTEN*$^{+/-}$ megalencephaly (Case A2).

Other CSF–Brain Interfaces Are Also Damaged in ASD

Patches of decreased neuronal gene expression have been reported in upper cortical layers of ASD postmortem brains,[10] so we examined the upper cortical layers in these ASD brains for evidence of pathology. The neuropil (neuronal processes) of cortical layer I was depleted in a patchy distribution associated with increased GFAP$^+$ staining of subpial astroglia in the ASD cases (not shown). Overlying the pial surface, we observed focal increases of leptomeningeal perivascular lymphocytes and focal collections of GFAP$^+$ membranous blebs in the subarachnoid space similar to those found in the white matter perivascular spaces in ASD cases (Fig 7A), suggesting a possible cause of the focal neuropil loss. We quantified the subpial neuropil density from the pial surface through cortical layer I (normalized to neuropil density in deeper cortical layer IV) at the most severely affected regions in ASD and control cases. Neuropil density was reduced in ASD relative to controls in patches running 60 to 360μm below the pial surface (see Fig 7B), a location known to contain cortical pyramidal neuron apical dendrites, specialized GABAergic neurons, and various axonal afferent fibers and synapses.

Consistent with an effect of this inflammatory process on additional CSF–brain barriers (ventricle and pia) in ASD, we observed the following additional pathological lesions: (1) focal ependymal cell loss with astroglial scars protruding into the ventricular space lumen (granular ependymitis) and buried ependymal canals (see Fig 7C), (2) focal subpial mineral deposition (not shown), and (3) focal tufts of subpial astrogliosis (not shown). Only 2 ASD cases contained rare microglial nodules targeting neurons in gray matter (not shown).

Discussion

We report rare scattered, but prominent, perivascular lymphocytic infiltrates and associated astrocyte blebs within the Virchow–Robin and subarachnoid CSF spaces in a large proportion of ASD cases across a wide range of ages (5–68 years). The lymphocyte cuffs contain cytotoxic effector molecule granzyme B and an admixture of cell types including CD8$^+$ and CD4$^+$ T cells, rare CD20$^+$ B cells, and CD68$^+$ macrophages. In some foci, CD8$^+$ and CD4$^+$ T lymphocytes extend individually into the white and gray matter parenchyma (not shown). The larger lymphocytic cuffs sometimes contain CD20$^+$ B cells, presumably representing transient immature tertiary lymphoid organs as reported in multiple sclerosis,[11] which were often separate from the sites of astrocyte debris with associated CD8$^+$ cytotoxic T lymphocytes. The increased collagen deposition and expanded perivascular spaces with jagged contours in ASD suggest a destructive effect of the elevated cytotoxic T lymphocytes. The numbers of perivascular lymphocytes and the amount of GFAP$^+$ debris correlated across ASD cases (see Fig 2C), a finding that

FIGURE 5: Increases of perivascular space (with jagged contours) and lymphocyte count separate autism spectrum disorder from control cases. (A) A gallery of photomicrographs of white matter blood vessels from a control case (top row), and 3 autism cases (bottom 3 rows) stained with hematoxylin and eosin and Luxol fast blue, with computer-assisted segmentations of perivascular area highlighted in yellow, highlights the increased perivascular area and jaggedness found in autism brain. (B) The jaggedness index (squared second derivative of perimeter normalized to area) of the perimeters of these spaces (perivascular parenchymal contours) is plotted for each measured white matter vessel in every autism and control case. Dots represent jaggedness index for the area surrounding a single vessel. Overlaid box-and-whisker plots represent the median, upper and lower quartile, and upper/lower quartile ±1.5*(interquartile range). Smoothed density plots for all cases are shown on the right margin. X-axis labels are case names. The aggregate differences between autism and control counts are statistically significant ($p < 0.00001$; analysis of variance with Tukey post hoc comparison of means), as are the differences between genetic autism and control ($p = 0.00009$), and the difference between autism and genetic autism ($p = 0.002$; $n_{vessels}$[autism] = 238, $n_{vessels}$[control] = 150, $n_{vessels}$[genetic autism] = 50). (C) The aggregate difference between the absolute perivascular spaces measured in autism cases was higher than in control cases, with individual genetic autism cases spanning the range. Bar heights represent mean, and whiskers represent standard error of the mean. *$p < 0.05$, Welch *t* test. (D) A scatterplot of median lymphocyte count (data from Fig 3B) and median perivascular tissue damage (ie, jaggedness; data from B) for each autism and control case yields a clear separation. Marginal density plots for median lymphocyte count and median perivascular tissue damage are shown in the right and top subpanels, respectively.

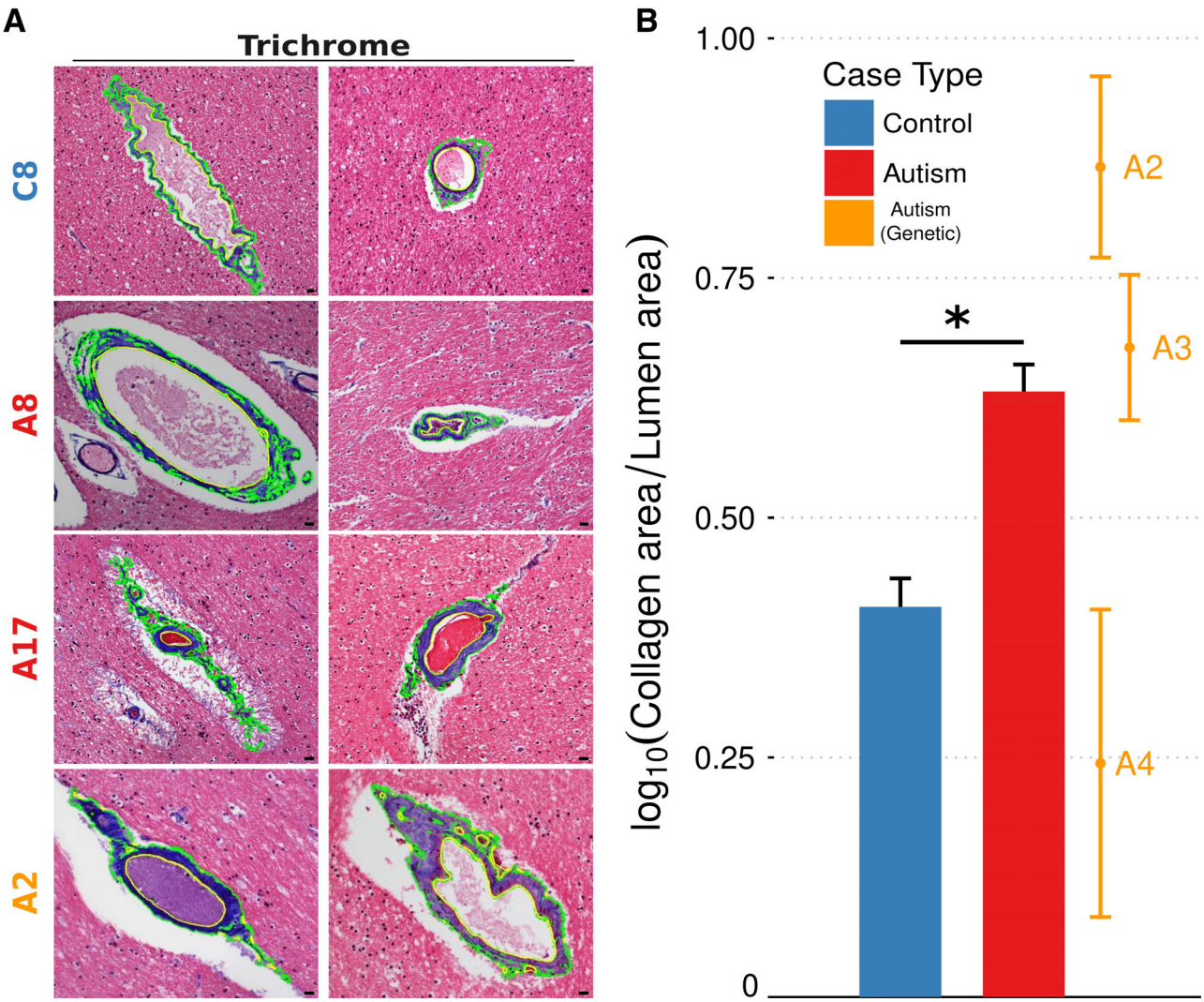

FIGURE 6: Increased perivascular collagen in autism spectrum disorder brains. (A) A gallery of photomicrographs of white matter blood vessels from a control case (top row), and 3 autism cases (bottom 3 rows) stained with trichrome, with computer-assisted segmentations of blue collagen highlighted in green, highlights the increased perivascular collagen found in autism cases. (B) The amount of perivascular collagen in white matter for each measured vessel in every case, normalized to the area of the vessel lumen, is higher across autism cases compared to controls. The aggregate differences between autism and control counts are statistically significant (*$p < 0.00001$; analysis of variance with Tukey post hoc comparison of means), as is the difference between genetic autism and control ($p = 0.00003$), but not the difference between autism and genetic autism ($p = 0.88$; $n_{vessels}$[autism] = 120, $n_{vessels}$[control] = 134, $n_{vessels}$[genetic autism] = 18).

suggests cytotoxic T lymphocytes may generate the astrocyte membranous blebs. Membranous blebs (also called apoptotic bodies) are generated from cells targeted by cytotoxic agents such as granzyme B or tumor necrosis factor α released from T lymphocytes.[12]

Astrocyte-derived membranous blebs have not been observed in other CNS disorders, and we suggest they may be generated by a targeted attack of astrocyte processes by cytotoxic T lymphocytes specifically at the glia limitans surrounding blood vessels and other CFS–brain boundaries. Consistent with our findings of increased GFAP$^+$ astrocyte debris in perivascular Virchow–Robin space CSF in ASD, GFAP is elevated in CSF and serum in a large proportion of individuals with ASD.[13] The strong separation of ASD from control cases on a lymphocyte count versus jaggedness index scatterplot (see Fig 5D) and the correlation of lymphocyte count with astrocyte debris on a scatterplot of ASD cases (see Fig 2C) suggest these histologic features could be causally connected biomarkers of the ASD pathogenic process. Our findings suggest future diagnostic evaluations and research of ASD postmortem brains should examine the following: (1) perivascular CD8$^+$ T-lymphocyte infiltrates, (2) CSF–glia limitans barrier damage (including increased perivascular space and collagen deposition), and (3) GFAP$^+$ astrocyte membranous blebs in CSF space compartments.

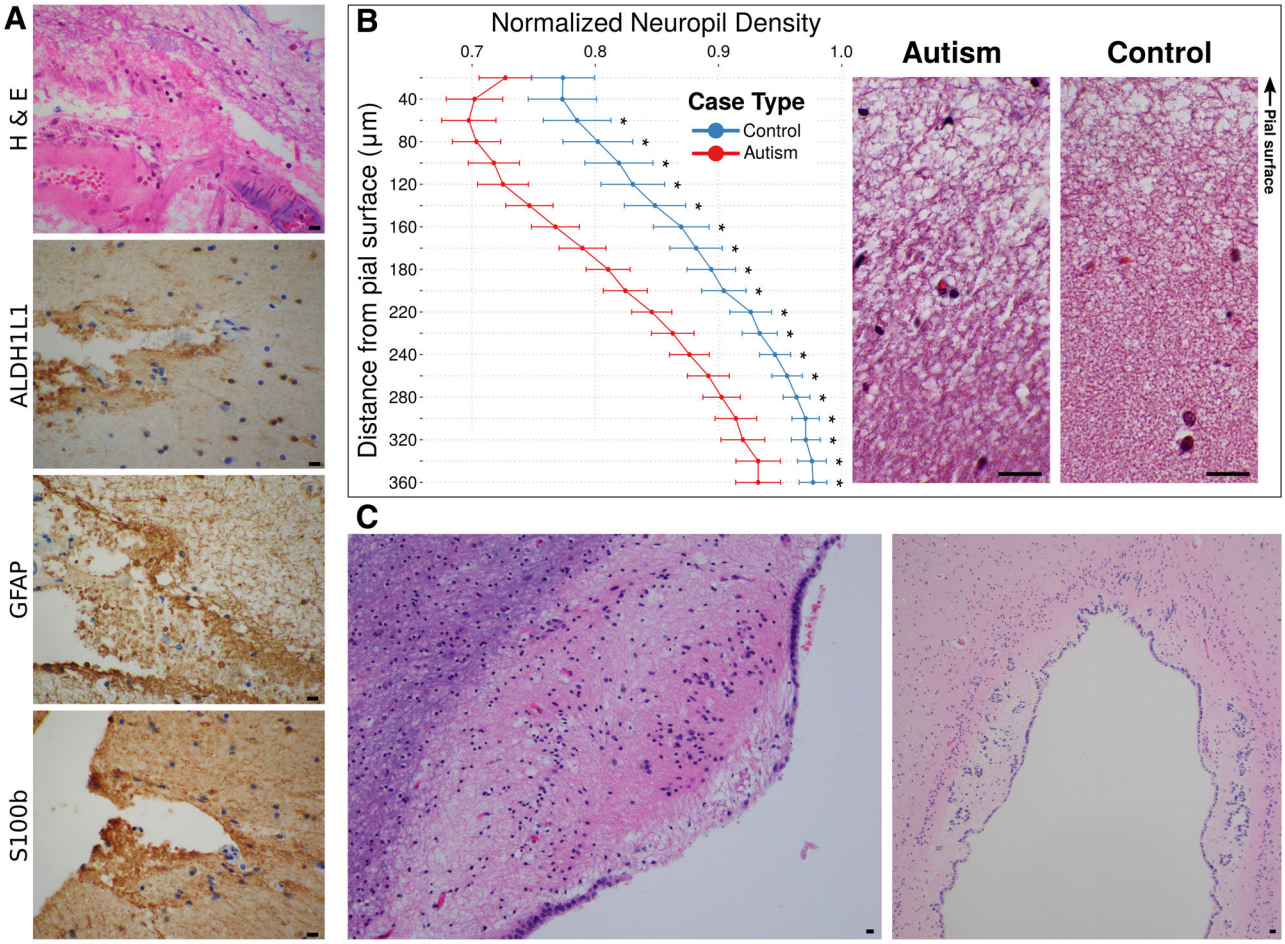

FIGURE 7: Rarefied cortical neuropil and leptomeningeal astroglial debris in autism. (A) Eosinophilic membranous debris can be seen in the leptomeningeal space between the pial surface and a leptomeningeal blood vessel (top; hematoxylin and eosin [H&E]). The debris stained positively on adjacent sections with antibodies to glial fibrillary acidic protein (GFAP), ALDH1L1, and S100b, confirming its astroglial origin (bottom 3 panels). All scale bars = 40µm. (B) Comparison of density of neuropil, excluding cell nuclei and normalized to density in an adjacent deep cortical layer on same slide, at increasing depth away from the pial surface shows rarefaction in the autism cases relative to controls (left). The vertical axis is aligned with the example images in the right panel. These images are coaligned such that the junction of pia and cortex forms the top border of the images. Reductions in density are observed at depths of 60 to 360µm in the autism cases. *$p < 0.05$, Welch t test with Bonferroni correction for multiple comparisons (n_{cases}[autism] = 24, n_{cases}[control] = 23). (C) In a subset of autism cases, the ependymal surface, another brain–cerebrospinal fluid interface, was damaged, showing granular ependymitis (left) and buried ependymal canals (example, cerebral aqueduct shown on right).

We suggest the invading $CD8^+$ lymphocytes in ASD may have T-cell receptors that selectively target epitope(s) presented by major histocompatibility complex (MHC)-expressing astrocytes localized at the glia limitans, where $CD8^+$ T-cell cytotoxic effectors such as granzyme B may be locally released to generate these $GFAP^+$ astrocyte membranous blebs in ASD. A magnetic resonance imaging study has revealed dilated Virchow–Robin spaces in the centrum semiovale white matter in 7 of 16 subjects with ASD,[14] a possible correlate to the dilated perivascular spaces we identified in white matter. Astrocyte debris released into the Virchow–Robin CSF spaces and leptomeningeal fibrosis (collagen deposition) could contribute to other brain pathologic processes such as the obstruction of CSF absorption consistent with the evidence of increased extra-axial CSF in high-risk infants who develop ASD.[15] The astrocyte-targeted damage could have direct or indirect (cytokine-mediated) immune effects on the ability of astrocytes to provide metabolic support to axons, causing action potential transmission failures,[16] as one explanation for the long-range functional connectivity deficits documented in ASD.[17]

This $CD8^+$ T-lymphocyte–rich immune neuropathology of ASD and that of other $CD8^+$ T-lymphocyte–rich immune disorders of the CNS are distinct in 2 ways: (1) the brain tissue compartments infiltrated by T lymphocytes and (2) the cell types attacked by the T lymphocytes. In multiple sclerosis, $CD8^+$ T lymphocytes are found in perivascular cuffs, but also extend more deeply into the white matter, where they attack oligodendrocytes to demyelinate axons and produce myelin debris.[18,19] In

Rasmussen encephalitis, $CD8^+$ T lymphocytes are found in perivascular cuffs, but also infiltrate cortical gray matter, where they attack and destroy pyramidal neurons.[20] ASD has $CD8^+$ T lymphocytes in brain perivascular cuffs, but has limited or no evidence of white matter demyelination, myelin debris, or cortical neuron destruction, and instead associates with $GFAP^+$ membranous bleb debris colocalized with and sometimes in continuity with the glia limitans perivascular astrocytes in ASD.

Analogous rare microscopic foci of activated immune cell attack occurs in polymyositis, an inflammatory myopathy of skeletal muscle that generates organ dysfunctions well beyond these microscopic foci. In addition to the minute foci of cytotoxic $CD8^+$ T-lymphocyte attack that generate myocyte necrosis, there are more widespread transcriptional changes including for example increased MHC class antigen expression and clinical evidence of muscle weakness.[21]

In type 1 diabetes (T1D), a $CD8^+$ T-lymphocyte autoimmune disorder of early childhood, specific MHC variants bind and present self-antigens to cytotoxic $CD8^+$ T cells to promote pancreatic islet cell destruction.[22,23] Like T1D, specific MHC alleles have been found in ASD.[24] Our data suggest these ASD-associated MHC alleles might play a role in presenting antigens to the $CD8^+$ T-lymphocyte infiltrates found in the ASD brain. T1D is initiated and possibly sustained by viral infections.[25] Although histologic evidence of typical CNS viral infections and immunohistochemical staining for herpes simplex virus 1 (HSV1), HSV2, varicella zoster virus, cytomegalovirus, and JC virus were negative (not shown), a potential role of infection in initiating or sustaining this T-lymphocyte immune response in ASD remains an important consideration.

Autism Cases A2 (*PTEN* megalencephaly) and A4 (XYY) were affected by the same T-lymphocyte and astroglial neuropathology as the idiopathic ASD cases. Importantly, *PTEN* heterozygosity is associated with lymphoid hyperplasia and an increased risk of autoimmune disease in human and mouse.[26,27] Similarly, XYY is a genetic defect reported in ASD cohorts,[28] and genes on the Y chromosome have been connected to an increased risk of immunologic disease.[29] By contrast, ASD Case A1 (mutations in *ARID1B*, *CACNA1C*, and *SLC6A8*), ASD Case A3 (mutation in *SETD2*), ASD Case A5 (dup15q), and another ~30% of the ASD cases that are genetically undefined lacked features of the T-lymphocyte and astroglial neuropathology, suggesting behavioral deficits in these genetic subsets of ASD might instead arise from direct effects of the genetic or epigenetic changes on the neuronal circuits controlling behaviors impaired in ASD.[30–36]

$CD8^+$ T-lymphocyte infiltrates and cytotoxic astrocyte membranous blebs represent a new cellular process not previously reported in studies of ASD neuropathology.[37–41] Future research should test whether the maternal–fetal[42–51] or autoimmune[52–55] antibodies found in the serum in some cases of ASD co-occur with the $CD8^+$ T-lymphocyte immune cell infiltrates and astrocyte membranous blebs or represent a separate autoimmune subtype of ASD. Autoantibodies, targeting multiple distinct pancreatic islet cell epitopes, co-occur with $CD8^+$ cytotoxic T-lymphocyte attack of islet cells in T1D.[23] Our study provides signature features of this T-lymphocyte immune subtype of ASD in postmortem cases and identifies astrocyte debris as a potential source of CSF or serum biomarkers for clinical diagnosis and monitoring of the pathology in living patients. Finally, with biomarkers that define the T-lymphocyte immune subtype of ASD, the efficacy of T-lymphocyte–targeted immunotherapies on biomarker levels and behavioral symptoms could be tested.

Acknowledgment

This study was supported by the Boston Children's Hospital Intellectual and Developmental Disabilities Research Center (U54 HD090255, P30 HD18655) and other funding to M.P.A. from the NIH National Institute of Mental Health (R01 MH114858, R01 MH112714), NIH National Institute of Neurological Disorders and Stroke (R01 NS08916), Nancy Lurie Marks Family Foundation, Landreth Foundation, Autism Speaks/National Alliance for Autism Research, and Simons Foundation/Autism BrainNet (FA#345171).

We thank Autism BrainNet, a resource of the Simons Foundation Autism Research Initiative, now including also Autism Speaks, Autism Tissue Program (ATP) collection; the families who donated tissue for research purposes to Autism BrainNet and the ATP; Dr J. Pickett, Dr C. M. Schumann, Dr C. A. Tamminga, Dr P. R. Hof, and C. K. Hare for their help in acquiring the brain samples and clinical details; and Drs P. R. Hof and K. Swanson for reading and editing the manuscript.

Author Contributions

M.M.D. and M.P.A. contributed to the conception and design of the study; all authors contributed to the acquisition and analysis of data; M.M.D. and M.P.A. contributed to drafting the text and preparing the figures.

Potential Conflicts of Interest

Nothing to report.

References

1. Vargas DL, Nascimbene C, Krishnan C, et al. Neuroglial activation and neuroinflammation in the brain of patients with autism. Ann Neurol 2005;57:67–81.
2. Laurence JA, Fatemi SH. Glial fibrillary acidic protein is elevated in superior frontal, parietal and cerebellar cortices of autistic subjects. Cerebellum 2005;4:206–210.
3. Morgan JT, Chana G, Pardo CA, et al. Microglial activation and increased microglial density observed in the dorsolateral prefrontal cortex in autism. Biol Psychiatry 2010;68:368–376.
4. Suzuki K, Sugihara G, Ouchi Y, et al. Microglial activation in young adults with autism spectrum disorder. JAMA Psychiatry 2013;70: 49–58.
5. Morgan JT, Barger N, Amaral DG, Schumann CM. Stereological study of amygdala glial populations in adolescents and adults with autism spectrum disorder. PLoS One 2014;9:e110356.
6. Garbett K, Ebert PJ, Mitchell A, et al. Immune transcriptome alterations in the temporal cortex of subjects with autism. Neurobiol Dis 2008;30:303–311.
7. Voineagu I, Wang X, Johnston P, et al. Transcriptomic analysis of autistic brain reveals convergent molecular pathology. Nature 2011; 474:380–384.
8. Gupta S, Ellis SE, Ashar FN, et al. Transcriptome analysis reveals dysregulation of innate immune response genes and neuronal activity-dependent genes in autism. Nat Commun 2014;5:5748.
9. Bankhead P, Loughrey MB, Fernández JA, et al. QuPath: open source software for digital pathology image analysis. Sci Rep 2017;7: 16878.
10. Stoner R, Chow ML, Boyle MP, Sunkin SM, Mouton PR, Roy S, Wynshaw-Boris A, Colamarino SA, Lein ES, Courchesne E. Patches of disorganization in the neocortex of children with autism. N Engl J Med. 2014;370(13):1209–1219.
11. Mitsdoerffer M, Peters A. Tertiary lymphoid organs in central nervous system autoimmunity. Front Immunol 2016;7:451.
12. Poon IK, Lucas CD, Rossi AG, Ravichandran KS. Apoptotic cell clearance: basic biology and therapeutic potential. Nat Rev Immunol 2014;14:166–180.
13. Esnafoglu E, Ayyildiz SN, Cirrik S, et al. Evaluation of serum neuron-specific enolase, S100B, myelin basic protein and glial fibrilliary acidic protein as brain specific proteins in children with autism spectrum disorder. Int J Dev Neurosci. 2017;61:86–91.
14. Taber KH, Shaw JB, Loveland KA, et al. Accentuated Virchow-Robin spaces in the centrum semiovale in children with autistic disorder. J Comput Assist Tomogr 2004;28:263–268.
15. Shen MD, Kim SH, McKinstry RC, et al. Increased extra-axial cerebrospinal fluid in high-risk infants who later develop autism. Biol Psychiatry 2017;82:186–193.
16. Wender R, Brown AM, Fern R, et al. Astrocytic glycogen influences axon function and survival during glucose deprivation in central white matter. J Neurosci 2000;20:6804–6810.
17. Rane P, Cochran D, Hodge SM, et al. Connectivity in autism: a review of MRI connectivity studies. Harv Rev Psychiatry 2015;23: 223–244.
18. Hauser SL, Bhan AK, Gilles F, et al. Immunohistochemical analysis of the cellular infiltrate in multiple sclerosis lesions. Ann Neurol 1986; 19:578–587.
19. Babbe H, Roers A, Waisman A, et al. Clonal expansions of CD8(+) T cells dominate the T cell infiltrate in active multiple sclerosis lesions as shown by micromanipulation and single cell polymerase chain reaction. J Exp Med 2000;192:393–404.
20. Bien CG, Bauer J, Deckwerth TL, et al. Destruction of neurons by cytotoxic T cells: a new pathogenic mechanism in Rasmussen's encephalitis. Ann Neurol 2002;51:311–318.
21. Dorph C, Englund P, Nennesmo I, et al. Signs of inflammation in both symptomatic and asymptomatic muscles from patients with polymyositis and dermatomyositis. Ann Rheum Dis 2006;65: 1565–1571.
22. Jerram ST, Leslie RD. The genetic architecture of type 1 diabetes. Genes (Basel) 2017;8. pii: E209.
23. Redondo MJ, Steck AK, Pugliese A. Genetics of type 1 diabetes. Pediatr Diabetes 2018;19:346–353.
24. Torres AR, Sweeten TL, Johnson RC, et al. Common genetic variants found in HLA and KIR immune genes in autism spectrum disorder. Front Neurosci 2016;10:463.
25. Allen DW, Kim KW, Rawlinson WD, Craig ME. Maternal virus infections in pregnancy and type 1 diabetes in their offspring: systematic review and meta-analysis of observational studies. Rev Med Virol 2018;28:e1974.
26. Di Cristofano A, Kotsi P, Peng YF, et al. Impaired Fas response and autoimmunity in Pten+/- mice. Science 1999;285:2122–2125.
27. Chen HH, Handel N, Ngeow J, et al. Immune dysregulation in patients with PTEN hamartoma tumor syndrome: analysis of FOXP3 regulatory T cells. J Allergy Clin Immunol 2017;139:607–620.e15.
28. Tartaglia NR, Wilson R, Miller JS, et al. Autism spectrum disorder in males with sex chromosome aneuploidy: XXY/Klinefelter syndrome, XYY, and XXYY. J Dev Behav Pediatr 2017;38:197–207.
29. Teuscher C, Noubade R, Spach K, et al. Evidence that the Y chromosome influences autoimmune disease in male and female mice. Proc Natl Acad Sci U S A 2006;103:8024–8029.
30. Krishnan V, Stoppel DC, Nong Y, et al. Autism gene Ube3a and seizures impair sociability by repressing VTA Cbln1. Nature 2017;543: 507–512.
31. Smith SE, Zhou YD, Zhang G, et al. Increased gene dosage of Ube3a results in autism traits and decreased glutamate synaptic transmission in mice. Sci Transl Med 2011;3:103ra97.
32. Peca J, Feliciano C, Ting JT, et al. Shank3 mutant mice display autistic-like behaviours and striatal dysfunction. Nature 2011;472: 437–442.
33. Penagarikano O, Abrahams BS, Herman EI, et al. Absence of CNTNAP2 leads to epilepsy, neuronal migration abnormalities, and core autism-related deficits. Cell 2011;147:235–246.
34. Clement JP, Aceti M, Creson TK, et al. Pathogenic SYNGAP1 mutations impair cognitive development by disrupting maturation of dendritic spine synapses. Cell 2012;151:709–723.
35. Han S, Tai C, Westenbroek RE, et al. Autistic-like behaviour in Scn1a +/- mice and rescue by enhanced GABA-mediated neurotransmission. Nature 2012;489:385–390.
36. Won H, Lee HR, Gee HY, et al. Autistic-like social behaviour in Shank2-mutant mice improved by restoring NMDA receptor function. Nature 2012;486:261–265.
37. Anderson MP. Autism spectrum disorders. In: Adle-Biassette BH, Golden J, eds. *Developmental neuropathology*. Hoboken, NJ: Wiley-Blackwell, 2018:477–495.
38. Pardo CA, Vargas DL, Zimmerman AW. Immunity, neuroglia and neuroinflammation in autism. Int Rev Psychiatry 2005;17:485–495.
39. Bauman ML, Kemper TL. Neuroanatomic observations of the brain in autism: a review and future directions. Int J Dev Neurosci 2005;23: 183–187.
40. Blatt GJ. The neuropathology of autism. Scientifica 2012;2012: 703675.
41. Hutsler JJ, Casanova MF. Review: Cortical construction in autism spectrum disorder: columns, connectivity and the subplate. Neuropathol Appl Neurobiol 2016;42:115–134.
42. Warren RP, Cole P, Odell JD, et al. Detection of maternal antibodies in infantile autism. J Am Acad Child Adolesc Psychiatry 1990;29: 873–877.

43. Dalton P, Deacon R, Blamire A, et al. Maternal neuronal antibodies associated with autism and a language disorder. Ann Neurol 2003; 53:533–537.

44. Braunschweig D, Ashwood P, Krakowiak P, et al. Autism: maternally derived antibodies specific for fetal brain proteins. Neurotoxicology 2008;29:226–231.

45. Zimmerman AW, Connors SL, Matteson KJ, et al. Maternal antibrain antibodies in autism. Brain Behav Immun 2007;21:351–357.

46. Singer HS, Morris CM, Gause CD, et al. Antibodies against fetal brain in sera of mothers with autistic children. J Neuroimmunol 2008;194:165–172.

47. Croen LA, Braunschweig D, Haapanen L, et al. Maternal mid-pregnancy autoantibodies to fetal brain protein: the early markers for autism study. Biol Psychiatry 2008;64:583–588.

48. Braunschweig D, Duncanson P, Boyce R, et al. Behavioral correlates of maternal antibody status among children with autism. J Autism Dev Disord 2012;42:1435–1445.

49. Rossi CC, Fuentes J, Van de Water J, Amaral DG. Brief Report: Antibodies reacting to brain tissue in Basque Spanish children with autism spectrum disorder and their mothers. J Autism Dev Disord 2014;44:459–465.

50. Brimberg L, Sadiq A, Gregersen PK, Diamond B. Brain-reactive IgG correlates with autoimmunity in mothers of a child with an autism spectrum disorder. Mol Psychiatry 2013;18:1171–1177.

51. Jones KL, Van de Water J. Maternal autoantibody related autism: mechanisms and pathways. Mol Psychiatry 2019;24:252–265.

52. Singer HS, Morris CM, Williams PN, et al. Antibrain antibodies in children with autism and their unaffected siblings. J Neuroimmunol 2006;178:149–155.

53. Goines P, Haapanen L, Boyce R, et al. Autoantibodies to cerebellum in children with autism associate with behavior. Brain Behav Immun 2011;25:514–523.

54. Wills S, Rossi CC, Bennett J, et al. Further characterization of autoantibodies to GABAergic neurons in the central nervous system produced by a subset of children with autism. Mol Autism 2011; 2:5.

55. Quadros EV, Sequeira JM, Brown WT, et al. Folate receptor autoantibodies are prevalent in children diagnosed with autism spectrum disorder, their normal siblings and parents. Autism Res 2018;11: 707–712.

56. D'Gama AM, Pochareddy S, Li M, et al. Targeted DNA sequencing from autism spectrum disorder brains implicates multiple genetic mechanisms. Neuron 2015;88:910–917.